Long-wavelength polar optical modes in GaAs semiconductor layered structures

1993 J. Phys.: Condens. Matter 5 5389

(http://iopscience.iop.org/0953-8984/5/31/004)

J. Phys.: Condens. Matter 5 (1993) 5389–5400. Printed in the UK

Long-wavelength polar optical modes in GaAs semiconductor layered structures

R Pérez-Alvarez†§, F García-Moliner†, V R Velasco† and C Trallero-Giner‡

† Instituto de Ciencia de Materiales, CSIC, Serrano 123, 28006 Madrid, Spain

‡ Departamento de Física Teórica, Universidad de La Habana, San Lázaro y L, Ciudad Habana, Cuba

Received 1 April 1993, in final form 16 June 1993

Abstract. A long-wavelength model of polar optical modes coupling the vibration amplitude u (the relative displacement vector) and the electrostatic potential φ leads to a system of coupled differential equations. This system is here solved for a quantum well without approximations and with simultaneous satisfaction of mechanical and electrostatic matching boundary conditions. Explicit solutions for u and φ are given, and the resulting eigenmodes for GaAs-based quantum wells are studied in detail. The model gives modes with a mixed character describing the coupling between u and φ. Thus one single model yields confined quasi-longitudinal (strictly longitudinal for in-plane wavelength vector $\kappa = 0$), confined quasi-transverse (strictly transverse for $\kappa = 0$) and interface modes. The dynamical structure, spectral strength and spatial dependence of the relevant amplitudes are studied in detail. The results are in good agreement with available Raman experimental data and have all the basic features present in microscopic calculations. Some comments are made on the limitations of purely dielectric or purely mechanical models.

1. Introduction

Various problems of physical interest involving electron–polar-optical-phonon coupling in quantum wells and superlattices [1–3] require a reliable description of the polar optical modes in such structures. Lattice dynamics calculations based on fairly reliable microscopic models have been reported [4, 5]. Actually, available experimental data pertain to the long-wavelength limit and in fact, due to the characteristics of the Fröhlich-type interaction, real electron-phonon scattering—important as a mobility limiting factor—and polaron effects are also dominated by the long-wavelength limit. Hence, a substantial interest in obtaining a reasonable description in terms of a phenomenological long-wavelength—i.e. continuous—model has originated an abundant literature on the subject. Several theoretical proposals have been put forward [5–15] which represent widely different viewpoints and some have met with a degree of partial success.

Besides requiring a reasonable agreement with the results of reliable microscopic calculations, one should also require (i) theoretical consistency of the model and (ii) satisfactory agreement with the key features of experimental evidence. The theoretical issue concerns the matching boundary conditions at the interfaces and the field equation on which the analysis is based. In a problem involving a mechanical vibrational field and an

§ Permanent address: Departamento de Física Teórica, Universidad de La Habana, San Lázaro y L, Ciudad Habana, Cuba.

0953-8984/93/315389+12$07.50

electrostatic field, theoretical consistency requires mechanical continuity—i.e. continuity of vibration amplitudes and 'forces' [16] transmitted normally to the interfaces—and electrostatic continuity—i.e. continuity of the potential and of the normal component of the electric displacement vector. The most important type of experimental information comes from Raman scattering data, which provide direct information on the eigenmodes of the system under study. Data are available for a wide range of superlattices, especially GaAs related, and they suggest the existence of essentially two types of mode, namely those with amplitudes mainly concentrated in one of the constituent materials [17–19], which are usually termed confined modes, and those with amplitudes somewhat tending to concentrate at the interfaces [20, 21]. The character of these modes is inferred somewhat indirectly, as the Raman scattering data do not give the spatial dependence of the amplitudes. This point will be discussed later. However, the geometry of the Raman scattering experiment can be chosen [22] in such a way that modes with different symmetries can be selectively excited. This provides direct evidence on a key feature of the eigenmodes under study.

It is well known that models of the dielectric type achieve electrostatic continuity but at the expense of producing mechanical discontinuity. Moreover, the symmetry pattern is in contradiction with experimental evidence. On the other hand, models of a rather more 'hydrodynamic' type or similar achieve mechanical continuity and predict the correct symmetry pattern, but they yield a discontinuous electrostatic potential. Sometimes [5, 15] this is remedied by imposing artificially forced *ad hoc* matching conditions and in any case assuming a vibrational field which is purely longitudinal. The latter is actually an unjustified approximation, as the matching at the interface in general always mixes longitudinal and transverse polarizations [14, 23, 24]. The only case in which this decoupling is strictly correct is when $\kappa \simeq 0$.

A theoretical formulation which meets all requirements was discussed in [16] and it was shown that there is no incompatibility in achieving mechanical and electrical continuity simultaneously provided that (i) one keeps the vibrational field u quite general, as the sum of a longitudinal field $u_L(\nabla \wedge u_L = 0)$ and a transverse field $u_T(\nabla \cdot u_T = 0)$ and (ii) one takes full account of the coupling between the mechanical field u and the electrostatic potential φ. The purpose of the present paper is to solve fully the system of coupled differential equations derived in [16] and to give and discuss the explicit solutions for u and φ.

Section 2 summarizes the theoretical model and presents the method employed for solving the differential system, as well as the fitting procedure for the input parameters used in the calculations. Some selected results are presented in section 3 for a GaAs-based quantum well and final comments are made in section 4.

2. Theoretical and practical aspects of the model

Let us consider a medium where $u(r, t)$ is the relative displacement and $\varphi(r, t)$ is the scalar potential associated with the electric field $E = -\nabla\varphi$. In the long wavelength phenomenological model we have a mechanical equation of motion for u which is of the form

$$\rho(\omega^2 - \omega_{TO}^2)u + \nabla \cdot \tau - \alpha\nabla\varphi = 0 \qquad \alpha^2 = \omega_{TO}^2\rho(\epsilon_0 - \epsilon_\infty)/4\pi. \tag{1}$$

The harmonic oscillator part is contained in the first term. The second term has the nature of a dispersive mechanical term and for an isotropic medium is of the form

$$\tau_{ij} = -\rho(\beta_L^2 - 2\beta_T^2)\delta_{ij}\nabla \cdot u - \rho\beta_T^2(\nabla_i u_j + \nabla_j u_i) \tag{2}$$

where $\nabla_i = \partial/\partial x_i$ and β_L and β_T are adjustable parameters. The sign of (2) is opposite to the usual one for acoustic waves on account of the negative dispersion of the optical modes. Crystalline anisotropy can be equally included but here we shall discuss the isotropic case [25]. The third term measures the effect of the coupling between the u and φ fields on the equation of motion for u—a factor ρ is missing in [16] in the definition of α^2. Simultaneously we have a Poisson equation for φ which reads [16]

$$\nabla^2\varphi = 4\pi\gamma\nabla\cdot u \qquad \gamma = \alpha/\epsilon_\infty. \tag{3}$$

The physical meaning of this is that φ is created by the polarization charge $\rho_p = \nabla\cdot P$ of the polarization field given by:

$$P = \alpha u + [(\epsilon_\infty - 1)/4\pi]E = \alpha u - [(\epsilon_\infty - 1)/4\pi]\nabla\varphi. \tag{4}$$

The term on the RHS of (3) measures the effect of the coupling between the φ and u fields on the field equation for φ. Of course we are working in the quasi-static limit ($c \to \infty$) which is fully justified for the situation under study.

The situation is similar to that of the theory of piezoelectric waves, as indeed was originally stressed by Born and Huang [26] and the only general way to obtain a correct solution is to solve the simultaneous set of four coupled differential equations. For an isotropic bulk homogeneous medium it is possible to obtain independent equations for u_L and u_T and this yields at once decoupled longitudinal and transverse modes with dispersion relations

$$\omega_L^2 = \omega_{LO}^2 - \beta_L^2 k^2 \qquad \omega_T^2 = \omega_{TO}^2 - \beta_T^2 k^2 \tag{5}$$

where k is the 3D wavevector and $\omega_{LO}^2 = \omega_{TO}^2(\epsilon_0/\epsilon_\infty)$. However, our concern is to study the matching of different media at an interface and then to apply this to the study of a quantum well structure. For layered structures (1) and (3) should be solved within each layer and the solutions appropriately matched at the interfaces.

Let us first discuss one interface which we take as the plane $z = 0$. We first Fourier transform in the 2D plane of the interface, so that the ω-dependent vibration amplitudes are of the form

$$u(\rho, z) = \exp(i\kappa\cdot\rho)u(z) \tag{6}$$

where κ, ρ are 2D vectors (wavevector and position) respectively.

We proceed likewise for φ and concentrate on $u(z)$ and $\varphi(z)$. These are (ω, κ)-dependent quantities for which, after 2D Fourier transform, we have (ω, κ)-dependent differential equations in the independent variable z. We stress that in general u consists of u_L and u_T.

The matching boundary conditions were obtained in [16] and [25] and they are, in the variable z,

$$\begin{aligned} &u_j(+0) = u_j(-0) \qquad \varphi(+0) = \varphi(-0) \qquad \tau_{zj}(+0) = \tau_{zj}(-0) \\ &z = \pm 0 \qquad \epsilon_\infty d\varphi/dz - 4\pi\alpha u_z = \text{continuous.} \end{aligned} \tag{7}$$

On evaluating these expressions at $z = \pm 0$ we must account for the different values of β_L, β_T, ϵ_∞ and α on both sides of the interface.

We have four amplitudes (u_x, u_y, u_z, φ), four coupled second order linear differential equations and eight matching boundary conditions. As in the study of piezoelectric surface or interface waves [27] it proves convenient to define a tetrafield

$$F \equiv \begin{bmatrix} F_M \\ F_E \end{bmatrix} \equiv \begin{bmatrix} u \\ \varphi \end{bmatrix} \tag{8}$$

which has mechanical and electrical components and to condense the system (1), (3) in the form

$$L \cdot F = 0 \tag{9}$$

where L is a 4×4 differential matrix which can be readily written down explicitly. Upon 2D Fourier transformation L depends on κ (ω-dependence understood everywhere) and contains the differential operator d/dz. A convenient technique for solving this problem is the surface Green function matching (SGFM) method [24].

For each bulk constituent medium one studies the compact differential system (9) and defines the corresponding bulk Green function G. After 2D Fourier transformation we have, for given ω,

$$L(\kappa, z)G(\kappa; z - z') = I_F \delta(z - z') \tag{10}$$

where I_F is the 4×4 unit matrix which, as in the study of piezoelectric interface waves [24, 27] consists of a 3×3 'mechanical unit' matrix I_M and of the 'electrical unit' I_E. Thus

$$I_F = \begin{Vmatrix} I_M & 0 \\ 0 & I_E \end{Vmatrix} = \begin{Vmatrix} 1 & 0 & 0 & 0 \\ 0 & 1 & 0 & 0 \\ 0 & 0 & 1 & 0 \\ 0 & 0 & 0 & 1 \end{Vmatrix}. \tag{11}$$

After full 3D Fourier transformation we have

$$L(\kappa, k_z) \cdot G(\kappa, k_z) = I_F. \tag{12}$$

The problem is then one of ordinary matrix algebra. Inversion of the matrix $L(\kappa, k_z)$ yields the matrix $G(\kappa, k_z)$. It can then be used for the SGFM calculation where the matching boundary conditions (7) are expressed in terms of the corresponding Green function matrix elements and derivatives thereof [24].

For the isotropic case we can choose $\kappa = (0, \kappa)$ in the y-direction without loss of generality. We then find

$$L_{12} = L_{13} = L_{14} = L_{21} = L_{31} = L_{41} = 0 \tag{13}$$

so the element

$$L_{11}(\kappa, k_z) = \rho(\omega^2 - \omega_{TO}^2) + \rho\beta_T^2(\kappa^2 + k_z^2) \tag{14}$$

factorizes out of the full $L(\kappa, k_z)$ matrix, leaving us with the inversion of a 3 × 3 matrix of elements

$$\begin{aligned}
L_{22} &= \rho(\omega^2 - \omega_{TO}^2) + \rho\beta_T^2(\kappa^2 + k_z^2) + \rho(\beta_L^2 - \beta_T^2)\kappa^2 \\
L_{33} &= \rho(\omega^2 - \omega_{TO}^2) + \rho\beta_T^2(\kappa^2 + k_z^2) + \rho(\beta_L^2 - \beta_T^2)k_z^2 \\
L_{23} &= L_{32} = +\rho(\beta_L^2 - \beta_T^2)\kappa k_z \\
L_{24} &= -(\epsilon_\infty/4\pi)L_{42} = -i\alpha\kappa \\
L_{34} &= -(\epsilon_\infty/4\pi)L_{43} = -i\alpha k_z \\
L_{44} &= +(\kappa^2 + k_z^2).
\end{aligned} \tag{15}$$

Thus we have one transverse vibrational amplitude $u_x(z)\exp(i\kappa y)$, propagating in the y-direction, uncoupled to the rest—this will be discussed later—and two amplitudes $u_y(z)\exp(i\kappa y)$ and $u_z(z)\exp(i\kappa y)$ plus the electrostatic 'amplitude' $\varphi(z)\exp(i\kappa y)$, all three

coupled. The wave consists of *both* the mechanical and the electrostatic excitations mutually coupled. A full normal mode calculation yields the full three amplitudes $(F_2, F_3, F_4) = (u_y, u_z, \varphi)$ and, having obtained this, we can then study the mechanical $(\boldsymbol{u})$ and electrostatic (φ) amplitudes separately. In general the solutions of the 3×3 problem describe a mechanical wave $\boldsymbol{u}$ which is sagittal and has a longitudinal part $\boldsymbol{u}_L$ and a transverse part $\boldsymbol{u}_T$. The electrostatic potential φ and $\boldsymbol{u}_L$ are coupled by the matching boundary conditions to $\boldsymbol{u}_T$, thus an electrical vibration φ drives the full mechanical vibration $\boldsymbol{u}$ and vice versa.

The SGFM analysis yields the full Green function G_s of the matched system in terms of the bulk Green functions G_μ of the constituent media ($\mu = 1, 2$). From the full Green function G_s, we can obtain the dispersion relations $\omega(\kappa)$ and all spectral functions of interest, such as the local density of states LDOS. One way to obtain the eigenvalues $\omega(\kappa)$ is to calculate the roots of the matching secular determinant, which can be written down from the projection of the matched G_s at the interface. For given κ this yields a set of eigenvalues which, by varying κ, give the desired dispersion relations $\omega(\kappa)$ for the normal modes. An alternative procedure is to calculate from G_s the κ-resolved local density of states $N_s(\omega, \kappa, z)$ for any convenient value of z, for instance at the interface. The eigenvalues $\omega(\kappa)$ are then the frequencies at which the peaks in the density of states appear and the dispersion relations are obtained by varying κ. In practice this procedure has often proved more convenient than looking for roots of the secular determinant [28] and we have found this also to be the case in the present calculation. This has the additional advantage that one obtains in the process the mode density, which is often itself an object of interest.

The above analysis is extended to the simultaneous matching at two coupled interfaces at finite distance. For instance, in a quantum well with two interfaces which we can label l (left) and r (right), the central object is the supermatrix

$$\tilde{G}_s = \begin{Vmatrix} G_s(\mathrm{l},\mathrm{l}) & G_s(\mathrm{l},\mathrm{r}) \\ G_s(\mathrm{r},\mathrm{l}) & G_s(\mathrm{r},\mathrm{r}) \end{Vmatrix} \tag{16}$$

which contains the local projections at the two interfaces and the cross terms which embody the coupling of these. The physical quantities of interest can then be obtained from $\tilde{G}_s$ [24]. The algebra for the present calculations was carried out by means of MATHEMATICA [29], with which closed-form expressions are obtained for the elements of (16).

Since we have studied $Al_xGa_{(1-x)}As$–GaAs systems, some words about the fitting procedure employed to estimate the input parameters are in order. The mass density and the background dielectric constants were obtained from a linear interpolation of the values for the pure materials—AlAs and GaAs—according to the formulae [30]:

$$\begin{aligned} \rho(x) &= 5.36 - 1.60\,x \text{ (c.g.s.)} \\ \epsilon_0(x) &= 13.18 - 3.12\,x \text{ (e.s.u.)} \\ \epsilon_\infty(x) &= 10.89 - 2.73\,x \text{ (e.s.u.)}. \end{aligned} \tag{17}$$

However, this type of interpolation would not work for ω_{LO}, ω_{TO}, β_L and β_T. It has been strongly argued on the basis of experimental evidence [31] that the ternary compound $Al_xGa_{(1-x)}As$ can be described in the *two-mode model*. We shall adopt this viewpoint and comment later on it. It then follows that if we study the matching to GaAs we must assign to the ternary alloy the values of the frequencies for the LO and TO modes found experimentally for the GaAs-like modes in this alloy [31]

$$\begin{aligned} \omega_{LO,GaAs}(x) &= 292.37 - 52.83\,x + 14.44\,x^2 \\ \omega_{TO,GaAs}(x) &= 268.50 - 5.16\,x - 9.36\,x^2. \end{aligned} \tag{18}$$

Here and henceforth ω is always given in cm^{-1}.

The β_L and β_T parameters are not usually reported in the literature and they are not known for the different types of mode in alloys. We have estimated their values for the pure materials ($x = 0, x = 1$) from the experimental curves of [31].

We have also made the following assumption: for very low (high) concentrations of Al, that is for $x \simeq 0 (x \simeq 1)$, we take dispersion laws with $\beta = 0$ for the AlAs(GaAs)-like modes. This assumption relies on the fact that for these situations the atoms in question are isolated and their phonon branches must be flat. For a given concentration x, we perform a linear interpolation between the values for $x = 0$ and $x = 1$. With ω in cm^{-1}, β is dimensionless and we obtain

$$\beta^2_{L,GaAs}(x) = 2.91\ (1-x)\ 10^{-12} \qquad \beta^2_{T,GaAs}(x) = 3.12\ (1-x)\ 10^{-12} \quad (19)$$

This interpolation is admittedly gratuitous. In fact we tested that the values of these parameters are altogether rather unimportant.

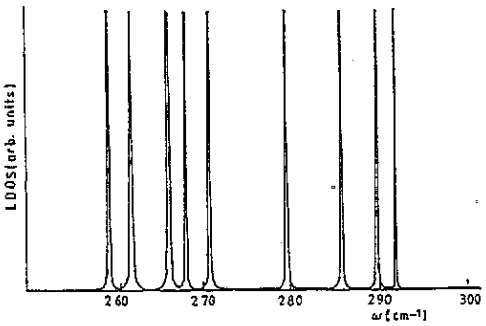

Figure 1. LDOS at the interfaces of the quantum well described in the text. LDOS in arbitrary units, $\kappa = 0$, ω in cm^{-1}. All subsequent figures pertain to the same well.

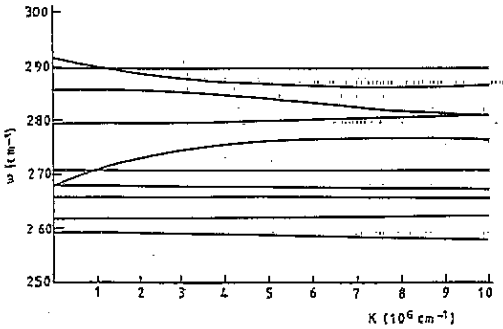

Figure 2. Dispersion relations for the eigenmodes obtained by starting from the eigenvalues (in cm^{-1}) of figure 1 and varying κ (in 10^6 cm^{-1}). Note the splitting of the degeneracy of the modes $m = 6$ and 7 for $\kappa \neq 0$. These two modes merge in one single peak in figure 1.

3. Results

In [18] a GaAs well of width $d = 20$ Å with $Al_{0.9}Ga_{0.1}As$ outside has been studied experimentally. We shall concentrate mainly on this well and characterize fully all the relevant physical features of the results. Figure 1 shows the (LDOS) at the l or r interface, covering the range from ω_{LO}(GaAs) down to below ω_{TO}(GaAs) for $\kappa = 0$. The actual calculations have in fact been performed for $\kappa = 10^{-3}$ cm^{-1} for simple reasons of computational convenience, but for all practical purposes this can be taken as $\kappa = 0$ and it will be henceforth indicated as such. A small imaginary part was added to ω, so δ-functions become in practice the peaks shown in the figure. By repeating the calculation for different values of κ we obtain the dispersion relations shown in figure 2. We label the different eigenmodes by a discrete label $m = 1, 2, \ldots$. We ascribe $m = 1$ to the highest mode, so m grows on decreasing frequency. For the first few values of m, in the range close to ω_{LO}(GaAs), the eigenvalues do not differ significantly from those obtained for the

rigid-barrier model [8] from the formula

$$\omega_m^2 = \omega_{LO}^2 - \beta_L^2 m^2 \pi^2 / d^2. \tag{20}$$

This will be commented on later.

There is also a continuum for much lower frequencies ($\omega \leq 255$ cm^{-1}) but this is just an artifact of the model in which a quadratic dispersion law gives a constantly decreasing frequency with no cut-off. These frequencies are outside the range of physical interest. The artificial DOS for these low frequencies does not affect the results in the range of physical interest.

We note that the modes $m = 6$ and 7 are degenerate when κ is strictly zero, but this is resolved even for very small values of κ. We have concentrated mainly on the range of κ from zero to values of the order of 10^7 cm^{-1}, which represents a very small fraction of the Brillouin zone and yet spans the range of physical interest. We stress that the labelling of the eigenmodes by increasing m on decreasing frequency holds for all κ, either before or after the crossovers seen in the figure.

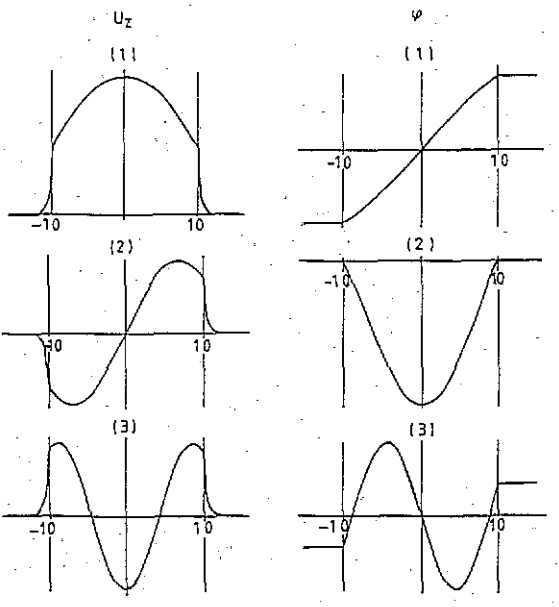

Figure 3. Spatial dependence of the mechanical (u_z: LHS) and electrical (φ: RHS) amplitudes for $\kappa = 0$, modes $m = 1, 2, 3$. The mode number is indicated in brackets and the abscissa z is in Å.

Firstly figure 3 gives the non-vanishing amplitudes as a function of z, for $\kappa = 0$, for the first three modes ($m = 1, 2, 3$). It was noted above that the amplitude u_x factorizes out. The calculation evaluates u_y—which turns out to vanish—and the mechanical (u_z) and electrical (φ) amplitudes, shown in the figure. Note that with the geometry here chosen the curl of $\boldsymbol{u}$ has the only non-vanishing component

$$(\nabla \wedge \boldsymbol{u})_x = \mathrm{i}\kappa u_z - \mathrm{d}u_y/\mathrm{d}z \tag{21}$$

while

$$\nabla \cdot \boldsymbol{u} = \mathrm{i}\kappa u_y + \mathrm{d}u_z/\mathrm{d}z. \tag{22}$$

With $u_y = 0$, which is the case in figure 3, only the first term on the RHS of (21) survives and this vanishes for $\kappa = 0$, while $\nabla \cdot \boldsymbol{u} \neq 0$ always. Thus these modes are longitudinal,

but this is strictly so only for $\kappa = 0$. Modes 4 and 5 follow the same pattern and need not be discussed.

The results shown in figure 3 are given in arbitrary units, so some words are in order concerning the normalization convention used here. This has been chosen so that the value of u_z at one of the interfaces—which we always take to be the r interface—is equal to unity for each mode, thus the amplitudes for the different modes are plotted with different scales. This is done to facilitate the visualization of the key features of the amplitudes displayed in the figure. In these units $\varphi_1(r) = 4 \times 10^{-5}$, $\varphi_2(0) = -3 \times 10^{-5}$ and $\varphi_3(r) = 3 \times 10^{-6}$. To put it more intuitively, when $u_z(r) = 0.01$ Å for $m = 1$, then $e\varphi(r) \simeq 280$ meV, while for $m = 2$ $e\varphi(0) \simeq 210$ meV when $u_z(r) = 0.01$ Å, in line with the predominantly electrical character of mode $m = 1$, as will be discussed presently. The latter results for the frequency eigenvalues are in good agreement with experimental data [18]. There is a small systematic difference in the absolute values, which could be easily accounted for by a small inaccuracy in the determination of the well width. The symmetry pattern—for instance the parity of the electrostatic potential—follows the sequence odd ($m = 1$)/even ($m = 2$)/odd ($m = 3$)/... and the values of φ outside the well vanish for the even modes and are nonvanishing constants for the odd ones. These facts are in agreement with experimental evidence [18], as well as with the results of microscopic calculations [4, 5] and even with those obtained from a rigid-barrier model [8].

We also note that the vibration amplitude u_z in figure 3 does not vanish at the interfaces, where its magnitude is actually quite significant, again in agreement with microscopic calculations [4, 5]. Outside the interfaces u_z decreases very fast, typically over a distance of a few Å, and then vanishes. This is interestingly related to the nature of the model and bears out the fact that it is not only the matching boundary conditions that matter, but also the mathematical structure of the differential operator. By keeping both fields (u and φ) in the 4×4 differential system, the differential operator—for given ω, κ and as a function of k_z—has the two types of pole, namely (a) those of an electrical nature, at $k_z = \pm i\kappa$, and (b) those of a mechanical nature, at $k_z = \pm Q_L$ and $k_z = \pm Q_T$, where

$$Q_{L,T} = \left\{\kappa^2 + \left[\omega^2 - \omega_{LO,TO}^2\right]/\beta_{L,T}^2\right\}^{1/2}. \tag{23}$$

The former give spatially dependent amplitudes that go as $\exp(-\kappa|z|)$, which do not decay for $\kappa = 0$, while the latter give outside the well a spatial decay going as $\exp\left\{-Q_{L,T}|z|\right\}$, if z is measured from the interface one studies. The fast decay of u_z outside the interfaces seen in figure 3 is due to this and has a decay length of the order of $1/Q_L$, since the modes are purely longitudinal.

Let us discuss the crossover of modes 1 and 2 in figure 2. For $\kappa < \kappa_c$ (the crossover value of κ) the first mode is the more dispersive, while for $\kappa > \kappa_c$ the more dispersive branch has become the mode $m = 2$. The clearest way to characterize these modes is to separate out from the LDOS the spectral strengths corresponding to the electrical and mechanical excitations. In the present calculation this is done by separating out the contribution of the fourth diagonal element of the Green function G_s. Figure 4 presents the electrical and mechanical spectral strengths for the first two modes in the neighbourhood of κ_c. Figures 4(a) and 4(b) are given for $\kappa < \kappa_c$ while 4(c) and 4(d) correspond to $\kappa > \kappa_c$. It can be seen from figure 4 that the first mode for low values of κ is mainly due to the electrical pole, while the second mode is mostly mechanical in origin, nevertheless both have a mixed character. In contrast, for $\kappa > \kappa_c$, the first mode is mostly mechanical—figure 4(d)—while the second mode is mostly electrical—figure 4(c).

The changes in the character of the modes can be further seen by comparing figures 3 and 5. The latter shows u_z and φ as function of z for $m = 1, 2, 3$, when $\kappa > \kappa_c$. There

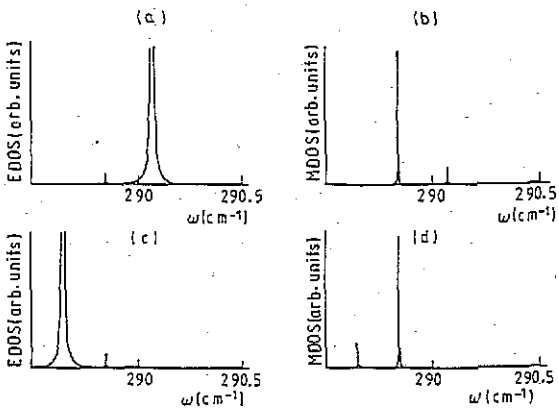

Figure 4. Electrical (a, c) and mechanical (b, d) spectral strengths for the upper and lower modes in the immediate neighbourhood of the crossover between modes $m = 1$ and $m = 2$. $\kappa = 1.1 \times 10^6$ cm^{-1} for (a, b) and $\kappa = 1.4 \times 10^6$ cm^{-1} for (c, d). Spectral strengths are in arbitrary units and ω in cm^{-1}.

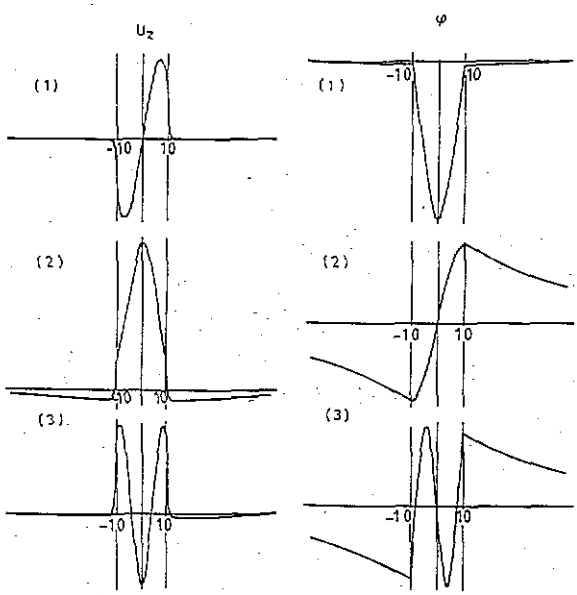

Figure 5. As figure 3, for $\kappa = 2 \times 10^6$ cm^{-1}, with z extending up to ± 60 Å.

is a small $|u_y| \ll |u_z|$ which is not displayed. Explicit evaluation shows that $|\nabla \wedge \boldsymbol{u}|$ is still much smaller than $|\nabla \cdot \boldsymbol{u}|$, so these modes are still in practice quasi-longitudinal for this low value of κ. The amplitudes are shown again in different scales, so that the key features can be visualized. The comments and conventions made in connection with figure 3 also apply here. In particular, $u_z(r)$ is always equal to unity and then, in these units, $\varphi_1(0) = -2.6 \times 10^{-5}$, $\varphi_2(r) = 7.6 \times 10^{-5}$ and $\varphi_3(r) = 6.0 \times 10^{-6}$.

The information in figures 3, 4 and 5 shows how the parity of φ and the predominance of electrical or mechanical character are interchanged at $\kappa = \kappa_c$. If E/O denotes even/odd z-dependence, then the parity sequence for φ_1 to φ_5 is O, E, O, E, O when $\kappa < \kappa_c$ and it changes to E, O, O, E, O when $\kappa > \kappa_c$. This range appears to be experimentally inaccessible to

Raman scattering, but the analysis suggests that a careful description of the mixed character of the normal modes of the 4×4 differential system is necessary in order to have a firm theoretical basis for the study of the electron–phonon coupling when not so small values of κ are involved, as may be the case with mobility calculations. The point is that the electronic wavefunctions in a symmetric quantum well have definite parities.

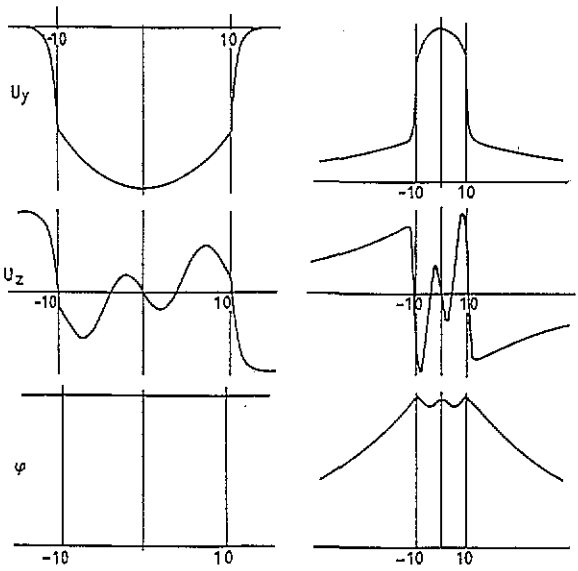

Figure 6. This figure describes the nature of the mode having predominant electrical character before and after the crossover of branches 5 and 6 of figure 2. The mechanical and electrical amplitudes on the left are for $\kappa = 10$ cm^{-1} and correspond to the mode $m = 6$, while on the right they are for $\kappa = 2 \times 10^6$ cm^{-1} and correspond to the mode $m = 5$. Note the different scales for z which ranges between ±15 Å on the left and ±60 Å on the right.

Now, it can be seen from figure 2 that there are two very dispersive modes. The mode $m = 6$ (starting from $\kappa = 0$) originates the second crossover with mode $m = 5$ for low κ. The system of eigenmode branches presents two modes (for every κ) which have predominantly electrical character. These are $m = 1$ and $m = 6$ for $\kappa < \kappa_c$, while for $\kappa > \kappa_c$ they correspond to $m = 2$ and $m = 6$. In the case of modes 5 and 6 the electrical and mechanical spectral strengths are also transferred in the manner of figure 4. Figure 6 shows the spatial dependence of u_y, u_z and φ for κ before ($m = 6$) and after ($m = 5$) the crossover, that is, following on the predominantly electrical mode. We find that $u_y(z)$ and $\varphi(z)$ are even while $u_z(z)$ is odd in both cases. With the same units, conventions—$u_z(r) = 1$ always—and different scales as employed for figures 3 and 5, $u_y(r) = -1.3 \times 10^{-2}$ for $m = 6$ and $u_y(r) = 6.7 \times 10^{-6}$ for $m = 5$, while $\varphi(r) = 65.5$ for $m = 6$ and $\varphi(r) = 1.3 \times 10^{-4}$ for $m = 5$.

These results characterize the different eigenmodes by direct evaluation of several well defined physical features, avoiding the question of the names sometimes assigned to them, an issue which is far less significant and which often leads to semantic confusion. For instance, if we consider the two very dispersive modes we note that (i) the predominantly electrical character stays with them—meaning that we start with $m = 1$ or 6 and then follow with $m = 2$ or 5—and (ii) the electrostatic potential has a tendency to accumulate amplitude around the interfaces, and then decays exponentially outside the well. In figure 6, for instance, this is more visible in mode $m = 5$ because of the larger value of κ. Qualitatively

speaking mode 6 behaves in the same manner, but a small amplitude oscillation inside the well is not appreciable on the scale of the figure, and also the exponential decay is very slow for very small κ. Thus the modes having predominantly electrical character can be identified with the interface modes. The same calculation for just one interface yields only one such mode. When the symmetric quantum well is formed the two degenerate modes corresponding to the two interfaces split into the two interface modes of opposite parities. The consequence of the symmetry of the system is that each amplitude by itself has a definite parity. The vibration amplitude u_x is decoupled from the other amplitudes, and u_z, u_y and φ are related. The functions $u_y(z)$ and $\varphi(z)$ always have opposite parity to that of $u_z(z)$ (see figures 3, 5 and 6). We can compare the parities of different modes by referring only to the parity of one of the amplitudes, for which we choose $\varphi(z)$.

Now, if the modes were all purely longitudinal, then the first one would simply cross the second one, which has opposite parity, without mixing, while it would mix strongly with the third one which has again the same parity; the repulsion between the corresponding dispersion branches is clearly seen in figure 2. For $\kappa \neq 0$ the longitudinal and transverse parts are in principle coupled, and mode mixing takes place between modes 1 and 2 on one hand and 5 and 6 on the other hand. In the case of $\kappa \simeq \kappa_c$ a strong mixing of the longitudinal and transverse polarizations for $m = 5$ and $m = 6$ takes place, where the terms $|\nabla \wedge \boldsymbol{u}|$ and $|\nabla \cdot \boldsymbol{u}|$ are comparable. At $\kappa = 0$ mode 5 is totally longitudinal and mode 6 is totally transverse.

The modes $m = 7, 8, 9, 10$ are strictly transverse and purely mechanical for all κ, as they have only the amplitude u_x. The parity sequence of $u_x(z)$ for these modes is E, O, E,..., with very similar features and interpretation in terms of Q_T instead of Q_L (23).

4. Final comments

The main point of [16] was that a correct formulation of the phenomenological model for long wavelength polar optical phonons meets without contradiction all matching boundary conditions. For this it is essential to take proper account of the coupling between the $\boldsymbol{u}$ and φ fields. This paper bears this out by explicit solution of the 4×4 differential system which is required for a proper treatment of the two coupled fields.

The resulting waves, in the range of quasi-longitudinal modes, have therefore mixed nature and we have characterized this by evaluating the electrical and mechanical contributions to the total spectral strength. This bears out the transfer of character at the crossovers. The modes in this range are, as we have seen, quasi-longitudinal, but it is essential for a correct treatment of the problem to treat formally the full vector $\boldsymbol{u}$ as having longitudinal and transverse parts. This is particularly important in the range where mode 5, the lowest of the quasi-longitudinal modes, soon mixes very strongly with the initially transverse mode 6.

The model also gives the shear horizontal modes below the transverse threshold.

Furthermore, there are two very dispersive modes of predominantly electrical character—figure 2, modes $m = 1, 6$ for $\kappa = 0$—which cut across the others, originating crossovers with corresponding mode mixing. By studying the spatial dependence of $\varphi(z)$ we can identify at all κ the two modes, which are usually termed *interface modes*, for which the label m changes as κ increases and the corresponding crossovers take place.

Thus we have obtained a satisfactory theoretical basis for the study of electron–phonon interaction in quantum wells in terms of a comparatively simple phenomenological model.

Acknowledgments

This work was partly supported by the Spanish CICYT under Grant No MAT91-0738. One of the authors (RP-A) is indebted to the Spanish Ministry of Education and Science for the award of a Sabbatical Visiting Professorship, during which this work was done. We have benefited greatly from stimulating discussions with F Comas and M Cardona.

References

[1] Jusserand B and Cardona M 1989 *Light Scattering in Solids V* ed M Cardona and G Güntherodt (Heidelberg: Springer) p 49
[2] Menéndez J 1989 *J. Lumin.* **44** 285
[3] Fasolino A and Molinari E 1990 *Surf. Sci.* **228** 112
[4] Molinari E, Fasolino A and Kunc K 1986 *Superlatt. Microstruct.* **2** 393
Rücker H, Molinari E and Lugli P 1991 *Phys. Rev.* B **44** 3463; 1992 *Phys. Rev.* B **45** 6747
Molinari E, Baroni S, Giannozzi P and de Gironcoli S 1992 *Phys. Rev.* B **45** 4280
[5] Huang K and Zhu B 1988 *Phys. Rev.* B **38** 13 377
[6] Fomin V N and Pokatilov E P 1985 *Phys. Status Solidi* b **132** 69
[7] Babiker M 1986 *J. Phys. C: Solid State Phys.* **19** 683
[8] Trallero-Giner C and Comas F 1988 *Phys. Rev.* B **37** 4583
[9] Mori N and Ando T 1989 *Phys. Rev.* B **40** 617
[10] Popovic Z V, Cardona M, Richter E, Strauch D, Tapfer L and Ploog K 1990 *Phys. Rev.* B **41** 5904
[11] Bechstedt J and Gerecke H 1989 *Phys. Status Solidi* b **156** 151
[12] Enderlein R 1991 *Phys. Rev.* B **43** 14 513
[13] Ridley B K and Babiker M 1991 *Phys. Rev.* B **43** 9096
[14] Ridley B K 1991 *Phys. Rev.* B **44** 9002
[15] Zianni X, Butcher P N and Dharssi J 1992 *J. Phys.: Condens. Matter* **4** L77
[16] Trallero-Giner C, García-Moliner F, Velasco V R and Cardona M 1992 *Phys. Rev.* B **45** 11 944
[17] Tucker J E, Pinzuk A, Chemla D S, Gossard A C and Wiegmann W 1984 *Phys. Rev.* B **29** 7065
[18] Sood A K, Menéndez J, Cardona M and Ploog K 1985 *Phys. Rev. Lett.* **54** 2111
[19] Klein M V 1986 *IEEE J. Quantum Electron.* **QE-22** 1769
[20] Cardona M 1990 *Superlatt. Microstruct.* **7** 183
[21] Moubray D J, Cardona M and Ploog K 1991 *Phys. Rev.* B **43** 1598, 11 815
[22] Cardona M and Güntherodt G (ed) (1989) *Light Scattering in Solids (Topics in Applied Physics 66)* (Heidelberg: Springer)
[23] Landau L and Lifshitz E M 1970 *Theory of Elasticity (Course of Theoretical Physics 7)* (Oxford: Pergamon)
[24] García-Moliner F and Velasco V R 1992 *Theory of Single and Multiple Interfaces* (Singapore: World Scientific)
[25] Comas F and Trallero-Giner C 1993 *Physica* B+C (to be published)
[26] Born M and Huang K 1988 *Dynamical Theory of Crystal Lattices* (Oxford: Clarendon)
[27] Velasco V R 1983 *Surf. Sci.* **128** 117
[28] Muñoz M C, Velasco V R and García-Moliner F 1987 *Phys. Scr.* **35** 504; 1989 *Phys. Rev.* B **39** 1786
Brito-Orta R A, Velasco V R and García-Moliner F 1988 *Phys. Rev.* B **38** 9631
Colombo L, Miglio L, Brito-Orta R A, Velasco V R and García-Moliner F 1991 *J. Appl. Phys.* **70** 2079
[29] Wolfram S 1991 *MATHEMATICA. A System for Doing Mathematics by Computer* (Redwood City: Addison-Wesley)
[30] Adachi S 1985 *J. Appl. Phys.* **58** R1
[31] Wang Z P, Jiang D S and Ploog K 1988 *Solid State Commun.* **65** 661
[32] Dieulesaint E and Royer D 1990 *Elastic Waves in Solids* (New York: Wiley)